Slow light using excitonic population oscillation

Shu-Wei Chang and Shun-Lien Chuang*
Department of Electrical and Computer Engineering, University of Illinois at Urbana-Champaign, Urbana, Illinois 61801, USA

Pei-Cheng Ku and Connie J. Chang-Hasnian
Department of Electrical Engineering and Computer Science, University of California at Berkeley, California 94720, USA

Phedon Palinginis and Hailin Wang
Department of Physics, University of Oregon, Eugene, Oregon 97430, USA
(Received 15 December 2003; revised manuscript received 7 June 2004; published 22 December 2004)

We develop a theoretical model for slow light using excitonic population oscillation in a semiconductor quantum well. In a two-level system, if the resonant pump and the signal have a difference frequency within the range of inverse of the carrier lifetime, coherent population beating at this frequency will be generated. We analyze the excitonic population oscillation using an atomiclike model extended from semiconductor Bloch equations for both spin subsystems of the excitonic population and the electrical polarization density. The two spin subsystems are coupled by the excitation-induced dephasing rate, which depends on the net population difference in conduction and heavy hole quantized bands and the population exchange due to flip of the spins of electrons or holes. We present our theoretical results for the absorbance, the refractive index spectra, and the slowdown factor due to population oscillation at various pump intensities, and show very good agreement with experimental data. It is shown that a slowdown factor of 3.12×10^4 has been achieved for a semiconductor quantum-well structure. We also obtain analytical solutions from our theory and account for different response behaviors of the signal when its polarization is either parallel or orthogonal to that of the pump, which has also been confirmed by experiments.

DOI: 10.1103/PhysRevB.70.235333 PACS number(s): 78.67.De, 71.35.Gg, 73.21.Fg, 78.20.Ci

I. INTRODUCTION

Recently, the slowdown of a light pulse has been demonstrated by using electromagnetically induced transparency (EIT)[1–6] or population oscillation.[7] Group velocities as low as 8 and 57.5 m/s have been achieved by using EIT[5] and population oscillation,[7] respectively. In either case, the quantum coherence will induce a transparency window and a steep variation of the real part of the refractive index within a narrow frequency range. This steep variation can reduce the group velocity of the light pulse significantly if the carrier frequency of the light pulse lies within this frequency range. However, unlike the slow light via EIT which requires a long dephasing time, the slow light via population oscillation only requires a long relaxation time and is relatively easier to implement, especially in the material system with significant dephasing.

In a simple two-level system, if the dephasing time is much shorter than the relaxation time of the population difference, the coherent population beating induced by the frequency difference between the signal and the pump can create a dip in the absorption spectrum within a range of pump intensity. The corresponding refractive index dispersion will create a group velocity reduction at the dip of the absorption spectrum at zero signal-pump detuning.[8] Usually, the phenomenon of population oscillation is accompanied by four-wave mixing (FWM) because they emerge from the same origin—the beating caused by frequency difference between pump and signal. On the other hand, take resonant pump for example, if the relaxation time and the dephasing time are about the same, one will observe the triple absorption peaks resembling the optical Stark effect instead of the absorption dip.[9–11] The splitting will reflect the Rabi frequency of the pump. The short dephasing time is thus critical for the population oscillation.

Population oscillation in semiconductor lasers was discussed by Agrawal.[12] The quantum approach describing the nondegenerate four-wave mixing (NDFWM) in semiconductors has been explored in the case of quasiequilibrium by neglecting the Coulomb attraction between electrons and holes.[13] In semiconductor gain media, the many-body model of multiwave mixing including the population oscillation of total carrier density has also been discussed.[14] Recently, the excitonic population oscillation has also been successfully demonstrated by Ku *et al.*[15] In the experiment, a linearly polarized pump tuned to the resonance energy of the 1*s* heavy-hole (HH) exciton in quantum wells (QWs) is incident in the QW growth direction, as shown in Fig. 1. A weak signal with the polarization $\hat{e}_s$ either parallel or orthogonal to the polarization of the pump $\hat{e}_p$ propagates along with the pump to probe the variation of the absorbance and the phase delay induced by the pump. In semiconductor quantum structures, the effective dephasing time for the excitons is usually very short due to various scattering mechanisms caused by impurity, phonon, piezoelectricity, carrier-carrier scattering, size fluctuations of quantum structure, and so on.[16–20] However, under considerable carrier concentration due to optical excitation, the relaxation of net population difference, the difference between electron occupation in conduction (C) and HH subbands, is dominated by radiative recombination. The various scattering mechanisms exciting carriers from certain momentum states will contribute to the relaxation of

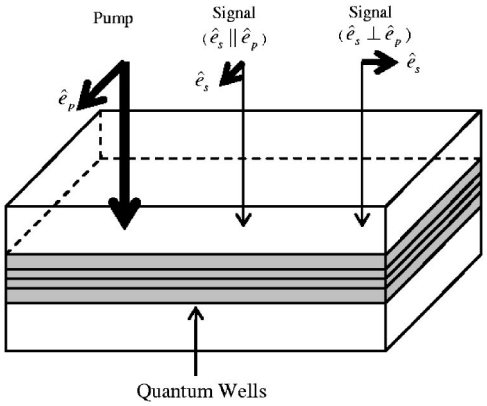

FIG. 1. Schematic diagram of the pump and signal polarizations for the parallel ($\hat{e}_p \| \hat{e}_s$) and orthogonal ($\hat{e}_p \perp \hat{e}_s$) configurations.

the total population into the reservoir. Physically, it corresponds to the diffusion of the excitons out of the area covered by the pump. If the fractional loss of the population due to diffusion out of the pump area is small, the main effect of the scattering is to redistribute the occupations in the phase space rather than affecting the relaxation time of the population difference significantly. In semiconductor QWs, although the radiative lifetime of excitons with zero center-of-mass momentum is about 10–30 ps, the distribution of the excitons in phase space will significantly increase the average value of radiative lifetime.[21–23] At low temperature, the average lifetime is usually in the order of several hundred picoseconds. In this way, the short dephasing time ranging from picoseconds to subpicoseconds and the much longer excitonic radiative recombination time, which is in the nanosecond range, can be utilized to demonstrate excitonic population oscillation in semiconductor quantum structures.

Unlike atomic gases or solid-state laser crystals, the structure and many-body effects in semiconductor quantum systems usually bring about various new phenomena absent in those cases. Among those observed phenomena, aside from the typical expectations of energy shift due to band-filling and reduction of the oscillation strength due to electron-hole plasma screening, the dephasing mechanisms can also exhibit observable features in absorption spectra.[24–26] The dephasing of the polarization in semiconductor quantum structures under intense pump cannot be simply described by a decay constant and is a contrast to the atomic case. A population dependence of dephasing, or so-called excitation induced dephasing (EID), has to be included. In semiconductors, the spin orientation of electrons and holes can only last for a finite period.[27–29] In addition to EID, the spin flip of electrons or holes in excitons can also influence the observed phenomena. Both EID and spin flip will cause different signal responses in the cases where the signal and pump polarizations are either parallel or orthogonal. Without EID and spin flip, the formulation of population oscillation will result in identical signal response for the two polarization configurations, which is a contradiction to the experiment. Polarization-dependent phenomenon is also present in the atomic case for EIT.[5] However, the origins of the phenomena are completely different in the cases of atomic gases and semiconductor quantum structures.

In Sec. II, we present our theoretical formulation starting from semiconductor Bloch equations for two spin subsystems of the 1*s* HH exciton in a QW. We then derive the coupled equations of polarization and excitonic population density by taking EID and spin flip into account. The polarization of the pump and signal fields as well as the selection rules of their corresponding transitions from HH subband to C subband are properly included in the dipole moments and their spin dependence. We then derive the complex permittivity function for the optical signal field in the presence of the pump. The refractive index change and the absorption spectrum caused by the population oscillation with a frequency determined by the signal-pump detuning is then derived. In Sec. III, we show our theoretical results for the absorption, the refractive-index spectra, the slowdown factor as a function of the pump-signal detuning, and their dependence on the polarization configurations, which cannot be simply explained by the usual theory of population oscillation. We then compare our theoretical results with the experimental data for a slowdown factor of 3.12×10^4 with very good agreement. We then summarize in Sec. IV.

II. FORMULATION

We start from semiconductor Bloch equations.[30,31] For simplicity, we neglect the Hartree-Fock energy shift caused by electron-electron as well as hole-hole interactions and the collision terms due to incoherent Coulomb interaction first. The relaxation of the population difference and the dephasing of the polarization will be included phenomenologically later. Also, only the first C-like and HH-like quantized bands are taken into consideration because they are the main contributors for the first discrete excitonic peak in the QW. We define the interband polarizations $P_{\mathbf{k},\sigma}$, carrier occupation numbers of electrons $n_{c,\mathbf{k},\sigma}$, and those of holes $n_{h,\mathbf{k},\bar{\sigma}}$ in the two-dimensional phase space of the two subsystems with spin indices $\sigma=\uparrow,\downarrow$ by the creation and annihilation operators of electrons $\alpha^{\dagger}_{\mathbf{k},\sigma}$, $\alpha_{\mathbf{k},\sigma}$ and holes $\beta^{\dagger}_{-\mathbf{k},\bar{\sigma}}$, $\beta_{-\mathbf{k},\bar{\sigma}}$

$$P_{\mathbf{k},\sigma}=\langle\beta_{-\mathbf{k},\bar{\sigma}}\alpha_{\mathbf{k},\sigma}\rangle, \tag{1a}$$

$$n_{c,\mathbf{k},\sigma}=\langle\alpha^{\dagger}_{\mathbf{k},\sigma}\alpha_{\mathbf{k},\sigma}\rangle, \tag{1b}$$

$$n_{h,\mathbf{k},\sigma}=\langle\beta^{\dagger}_{-\mathbf{k},\bar{\sigma}}\beta_{-\mathbf{k},\bar{\sigma}}\rangle, \tag{1c}$$

where $\mathbf{k}$ is the wave vector of the state; $\bar{\sigma}$ is the opposite spin projection of σ.

The coherent dynamics equations for the interband polarizations and carrier occupation numbers in phase space are then as follows:

$$\frac{\partial}{\partial t}P_{\mathbf{k},\sigma}=-\frac{i}{\hbar}(\epsilon_{c,\mathbf{k}}+\varepsilon_{h,\mathbf{k}})P_{\mathbf{k},\sigma}-i(n_{c,\mathbf{k},\sigma}+n_{h,\mathbf{k},\sigma}-1)\Omega_{\mathbf{k},\sigma}(t), \tag{2a}$$

$$\frac{\partial}{\partial t}n_{c,\mathbf{k},\sigma}=2\,\mathrm{Im}[\Omega^{*}_{\mathbf{k},\sigma}(t)P_{\mathbf{k},\sigma}], \tag{2b}$$

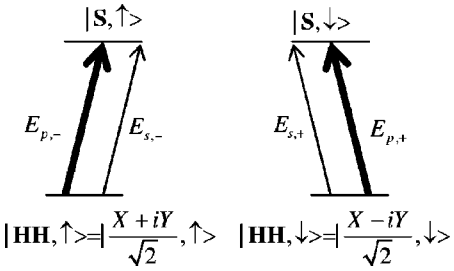

FIG. 2. The level configuration of the excitonic population oscillation. The positive-helicity components of the pump and signal as well as the spin-down C and HH bands consist of one subsystem while their counterparts form the other.

$$\frac{\partial}{\partial t} n_{h,\mathbf{k},\sigma} = 2\,\mathrm{Im}[\Omega^*_{\mathbf{k},\sigma}(t) P_{\mathbf{k},\sigma}], \tag{2c}$$

$$\Omega_{\mathbf{k},\sigma}(t) = \frac{1}{\hbar}\left[I_{ch} e\mathbf{r}_{ch,\sigma} \cdot \mathbf{E}(t) + \sum_{\mathbf{q}\neq\mathbf{k}} V_{|\mathbf{k}-\mathbf{q}|} P_{\mathbf{q},\sigma} \right], \tag{2d}$$

where $\epsilon_{c,\mathbf{k}}$ and $\epsilon_{h,\mathbf{k}}$ are the electron and hole energies, $\Omega_{\mathbf{k},\sigma}(t)$ is the time-dependent generalized Rabi frequency of the subsystem with spin σ, I_{ch} is the wave-function overlap integral between the quantized C-like and HH-like states along the growth direction, $e\mathbf{r}_{ch,\sigma}$ is the bulk interband dipole moment of the QW material, and V_q is the matrix element of the Coulomb potential in the phase space.

Following the procedure outlined in Ref. 31, we neglect the polarization parts of the generalized Rabi frequency when substituting Eq. (2d) into Eqs. (2b) and (2c) but keep them in Eq. (2a). This two-band model with sybsystems can be effectively transformed into two independent two-level subsystems if only the two lowest 1*s* HH excitons of opposite spins are included, as shown in Fig. 2. The quantities of interests in the excitonic population oscillation for this effective two-level model are the *effective polarizations* $P_{ex,\uparrow}$, $P_{ex,\downarrow}$ and the *effective population differences* between the higher and lower states $N_{ex,\uparrow}$, $N_{ex,\downarrow}$ of the two spin subsystems. The quantity $N_{ex,\sigma}$ is actually an analogy of the function $n_{c,\mathbf{k},\sigma}+n_{h,\mathbf{k},\sigma}-1$ in the phase space.

The electric field can be decomposed into two components:

$$\mathbf{E}(t) = \frac{1}{2}[\mathcal{E}(t) + \mathcal{E}^*(t)] \tag{3}$$

where $\mathcal{E}(t)$ contains the positive-frequency components while its complex conjugate contains the negative-frequency ones. Under rotating-wave approximation (RWA), the coherent dynamics equations of these quantities are as follows:

$$\frac{\partial P_{ex,\sigma}}{\partial t} = -\,i\omega_{ex} P_{ex,\sigma} - i\frac{I_{ch} e\mathbf{r}_{ch,\sigma} \cdot \mathcal{E}(t)}{2\hbar} N_{ex,\sigma}, \tag{4a}$$

$$\frac{\partial N_{ex,\sigma}}{\partial t} = 4\,\mathrm{Im}\left[\frac{I^*_{ch} e\mathbf{r}^*_{ch,\sigma} \cdot \mathcal{E}^*(t)}{2\hbar} P_{ex,\sigma} \right], \tag{4b}$$

where ω_{ex} is the resonant frequency of the 1*s* HH exciton.

The electric polarization density in real space can be written in terms of $P_{ex,\sigma}$:

$$\mathbf{P} = \frac{|\Phi_{ex}(\rho=0)|^2}{L_z} \sum_{\sigma} I^*_{ch} e\mathbf{r}^*_{ch,\sigma} P_{ex,\sigma}, \tag{5}$$

where $|\Phi_{ex}(\rho=0)|$ is the magnitude of the variational 1*s* excitonic in-plane wave function of the relative coordinate at origin,[32] and L_z is the width of QW.

Define the *effective total population difference* N_{ex}:

$$N_{ex} = N_{ex,\uparrow} + N_{ex,\downarrow}. \tag{6}$$

To account for the relaxation of the population differences, the exchange of the population difference between two subsystems, and the dephasing of the polarizations, the population relaxation constant Γ_1, the spin-flip constant Γ_s, and the polarization dephasing $\Gamma_2(N_{ex})$, which is a function of the effective total population difference N_{ex}, are inserted into equations (4a) and (4b):

$$\frac{\partial P_{ex,\sigma}}{\partial t} = -\,i[\omega_{ex} - i\Gamma_2(N_{ex})] P_{ex,\sigma} - i\frac{I_{ch} e\mathbf{r}_{ch,\sigma} \cdot \mathcal{E}(t)}{2\hbar} N_{ex,\sigma}, \tag{7a}$$

$$\frac{\partial N_{ex,\sigma}}{\partial t} = -\,\Gamma_1(N_{ex,\sigma} - N^{(0)}_{ex,\sigma}) - \Gamma_s(N_{ex,\sigma} - N_{ex,\bar{\sigma}}) + 4\,\mathrm{Im}\left[\frac{I^*_{ch} e\mathbf{r}^*_{ch,\sigma} \cdot \mathcal{E}^*(t)}{2\hbar} P_{ex,\sigma} \right], \tag{7b}$$

where $N^{(0)}_{ex,\sigma}$ is the respective effective population difference of the two subsystems in equilibrium, and $N_{ex,\bar{\sigma}}$ is the effective population difference with opposite spin index $\bar{\sigma}$. The quantity $N^{(0)}_{ex,\sigma}$ will be close to -1 no matter whether the intrinsic material is at room temperature or low temperature.

Equations (7a) and (7b) are actually only valid in the low-excitation regime. In this approximation, the effects of electron-hole-plasma screening and phase-space filling are not included. Therefore, the decrease of the oscillator strength and energy shift are beyond the scope of this model. However, due to the balance of band-gap shrinkage and the reduction of excitonic binding energy, the energy of the excitonic absorption peak does not shift much in a certain range of pump intensity.[31] We will show later that our model gives very good agreement with the experimental data.

For simplicity, we assume that the dependence of the relaxation constant Γ_1 and spin-flip constant Γ_s on the effective population difference is weak. Also, the relaxation constant Γ_1 is not directly related to the microscopic population relaxation of the states in the phase space. The microscopic intraband scattering makes the relaxation of a certain momentum state extremely fast. However, Γ_1 is a quantity describing the macroscopic population difference in C-like and HH-like subbands, which is determined mostly by radiative recombination in semiconductors. Typically, the average excitonic radiative lifetime at low temperature in direct-band-gap semiconductors is of the order of a nanosecond, which is long compared with subpicosecond intraband scattering times. On the other hand, the polarization dephasing does not have many distinctions between macroscopic and microscopic processes. Whatever contributes to the microscopic

dephasing can still show up in the current model. Therefore the polarization dephasing rate in the current model is much higher than the population relaxation rate.

The optical excitation will induce an effective population difference deviated from the one in equilibrium. It will bring about another contribution of dephasing due to exciton-exciton scattering or excitation induced dephasing. We adopt the following model:[24–26]

$$\Gamma_2(N_{ex}) = \Gamma_2^{(0)} + \gamma(N_{ex} - N_{ex}^{(0)}), \tag{8}$$

$$N_{ex}^{(0)} = N_{ex,\uparrow}^{(0)} + N_{ex,\downarrow}^{(0)}, \tag{9}$$

where $\Gamma_2^{(0)}$ is the intrinsic dephasing while γ is a phenomenological constant describing EID. The discussions and similar approximations can be found in the literature in order to explain the dependence of the experimental results on the pump-probe polarization configuration for FWM.[24–26,33] At very high excitation, the dependence of the dephasing on the population is not simply a linear relation. In that case, one can model the parameter γ as a function of the total effective population difference N_{ex}. However, to a first approximation, we take the parameter γ as a constant and will show that this approximation gives good agreement with experimental results. Without the constants γ and Γ_s, the total system is composed of two independent subsystems labeled by two spin indices. However, the existence of these two constants couples the two subsystems and thus complicates the whole problem.

Denote the QW plane as the $x-y$ plane. The positive-frequency part of the optical electric field is written as follows:

$$\mathcal{E}(t) = E_s e^{-i\omega_s t}\hat{e}_s + E_p e^{-i\omega_p t}\hat{e}_p, \tag{10}$$

where E_s and ω_s are the amplitude and frequency of the signal while E_p and ω_p are those of the pump. We assume that $|E_s|$ is much weaker than $|E_p|$. Although the spatial dependence is not explicitly shown in Eq. (10), we assume both the signal and pump are traveling along the growth direction (positive z direction) so that their electric fields can be decomposed into positive-helicity and negative-helicity components:

$$E_s\hat{e}_s = E_{s,+}\frac{\hat{x}+i\hat{y}}{\sqrt{2}} + E_{s,-}\frac{\hat{x}-i\hat{y}}{\sqrt{2}}, \tag{11a}$$

$$E_p\hat{e}_p = E_{p,+}\frac{\hat{x}+i\hat{y}}{\sqrt{2}} + E_{p,-}\frac{\hat{x}-i\hat{y}}{\sqrt{2}}, \tag{11b}$$

where $\hat{x}$ and $\hat{y}$ are the unit vectors along the x and y axes, respectively. The bulk dipole moments between C and HH subbands have similar forms due to their s-like ($|S,\uparrow\rangle$ and $|S,\downarrow\rangle$) as well as p-like ($|(X+iY)/\sqrt{2},\uparrow\rangle$ and $|(X-iY)/\sqrt{2},\downarrow\rangle$) periodic parts of Bloch wave functions, respectively,

$$e\mathbf{r}_{ch,\uparrow} = er_{ch}\frac{\hat{x}+i\hat{y}}{\sqrt{2}}, \tag{12a}$$

$$e\mathbf{r}_{ch,\downarrow} = er_{ch}\frac{\hat{x}-i\hat{y}}{\sqrt{2}}. \tag{12b}$$

We define the following Rabi frequencies corresponding to the positive-(negative-)helicity components for the signal and pump:

$$\Omega_{s,\pm} = \frac{I_{ch}er_{ch}E_{s,\pm}}{2\hbar}, \tag{13a}$$

$$\Omega_{p,\pm} = \frac{I_{ch}er_{ch}E_{p,\pm}}{2\hbar}. \tag{13b}$$

Due to the selection rule from the conservation of the total angular momentum along the growth direction, Equations (7a) and (7b) can be explicitly written as follows:

$$\frac{\partial P_{ex,\uparrow}}{\partial t} = -i[\omega_{ex} - i\Gamma_2(N_{ex})]P_{ex,\uparrow} - i(\Omega_{s,-}e^{-i\omega_s t} + \Omega_{p,-}e^{-i\omega_p t})N_{ex,\uparrow}, \tag{14a}$$

$$\frac{\partial N_{ex,\uparrow}}{\partial t} = -\Gamma_1(N_{ex,\uparrow} - N_{ex,\uparrow}^{(0)}) - \Gamma_s(N_{ex,\uparrow} - N_{ex,\downarrow}) + 4\,\mathrm{Im}[(\Omega_{s,-}^* e^{i\omega_s t} + \Omega_{p,-}^* e^{i\omega_p t})P_{ex,\uparrow}], \tag{14b}$$

$$\frac{\partial P_{ex,\downarrow}}{\partial t} = -i[\omega_{ex} - i\Gamma_2(N_{ex})]P_{ex,\downarrow} - i(\Omega_{s,+}e^{-i\omega_s t} + \Omega_{p,+}e^{-i\omega_p t})N_{ex,\downarrow}, \tag{14c}$$

$$\frac{\partial N_{ex,\downarrow}}{\partial t} = -\Gamma_1(N_{ex,\downarrow} - N_{ex,\downarrow}^{(0)}) - \Gamma_s(N_{ex,\downarrow} - N_{ex,\uparrow}) + 4\,\mathrm{Im}[(\Omega_{s,+}^* e^{i\omega_s t} + \Omega_{p,+}^* e^{i\omega_p t})P_{ex,\downarrow}]. \tag{14d}$$

In the later equations, the first spin index of $\uparrow$ ($\downarrow$) [or $\downarrow$ ($\uparrow$)] and the upper sign of $\mp$ (or $\pm$) appear in the same equation while the second spin index and the lower sign are present together. Equations (14a)–(14d) can be approximately solved by perturbation theory because of the weak signal. The basic approach follows from that by Boyd *et al.*[9] In typical population oscillation, a FWM signal should also be generated. However, we assume that the FWM signal itself is weak or the phase-matching condition is not fulfilled so that the FWM signal is not built up to feedback. The effective polarization and population difference can then be separated into parts corresponding to the signal and pump, respectively,

$$P_{ex,\uparrow(\downarrow)} = P_{ex,\uparrow(\downarrow)}^{(s)} + P_{ex,\uparrow(\downarrow)}^{(p)}, \tag{15a}$$

$$N_{ex,\uparrow(\downarrow)} = N_{ex,\uparrow(\downarrow)}^{(s)} + N_{ex,\uparrow(\downarrow)}^{(p)}. \tag{15b}$$

The parts $P_{ex,\uparrow(\downarrow)}^{(p)}$ and $N_{ex,\uparrow(\downarrow)}^{(p)}$ will provide the steady-state solution under intense pump. The intense pump causes

power-broadening for the two subsystems. We substitute Eqs. (15a) and (15b) into Eqs. (14a) as well as (14b) and then discard the signal terms. Under the standard procedures of density-matrix formulation, the steady-state part $P^{(p)}_{ex,\uparrow(\downarrow)}$ can be written as $\tilde{P}^{(p)}_{ex,\uparrow(\downarrow)}e^{-i\omega_p t}$, where $\tilde{P}^{(p)}_{ex,\uparrow(\downarrow)}$ is a slowly varying variable. The steady-state solution to this power-broadening phenomenon can be solved numerically by iteration:

$$\tilde{P}^{(p)}_{ex,\uparrow(\downarrow)} = \frac{\Omega_{p,\mp} N^{(p)}_{ex,\uparrow(\downarrow)}}{\omega_p - \omega_{ex} + i\Gamma_2^{(p)}}, \tag{16a}$$

$$N^{(p)}_{ex,\uparrow(\downarrow)} = \frac{\dfrac{\Gamma_s}{\Gamma_1}N^{(0)}_{ex} + \left(1 + \dfrac{4\Gamma_2^{(p)}|\Omega_{p,\pm}|^2/\Gamma_1}{(\omega_p - \omega_{ex})^2 + (\Gamma_2^{(p)})^2}\right)N^{(0)}_{ex,\uparrow\downarrow}}{\left(1 + \dfrac{2\Gamma_s}{\Gamma_1}\right) + \left(1 + \dfrac{\Gamma_s}{\Gamma_1}\right)\left[\dfrac{4\Gamma_2^{(p)}/\Gamma_1(|\Omega_{p,+}|^2 + |\Omega_{p,-}|^2)}{(\omega_p - \omega_{ex})^2 + (\Gamma_2^{(p)})^2}\right] + \left(\dfrac{4\Gamma_2^{(p)}/\Gamma_1|\Omega_{p,+}\Omega_{p,-}|}{(\omega_p - \omega_{ex})^2 + (\Gamma_2^{(p)})^2}\right)^2}, \tag{16b}$$

$$N^{(p)}_{ex} = N^{(p)}_{ex,\uparrow} + N^{(p)}_{ex,\downarrow}, \tag{16c}$$

$$\Gamma_2^{(p)} = \Gamma_2(N^{(p)}_{ex}) = \Gamma_2^{(0)} + \gamma(N^{(p)}_{ex} - N^{(0)}_{ex}). \tag{16d}$$

For convenience in the following derivations, we write the slowly varying part $\tilde{P}^{(p)}_{ex,\uparrow(\downarrow)}$ in terms of the newly defined functions $H_{\uparrow(\downarrow)}(\omega_p)$:

$$H_{\uparrow(\downarrow)}(\omega_p) = \frac{N^{(p)}_{ex,\uparrow(\downarrow)}}{\omega_p - \omega_{ex} + i\Gamma_2^{(p)}}, \tag{17a}$$

$$\tilde{P}^{(p)}_{ex,\uparrow(\downarrow)} = \Omega_{p,\mp}H_{\uparrow(\downarrow)}(\omega_p). \tag{17b}$$

After the steady-state parts have been obtained numerically, the dynamics equations related to the weak signal can be derived by comparing the terms of the signal up to the first order on the right-hand and the left-hand sides of Eqs. (14a) and (14b):

$$\frac{\partial P^{(s)}_{ex,\uparrow(\downarrow)}}{\partial t} = -i(\omega_{ex} - i\Gamma_2^{(p)})P^{(s)}_{ex,\uparrow(\downarrow)} - \gamma P^{(p)}_{ex,\uparrow(\downarrow)}(N^{(s)}_{ex,\uparrow} + N^{(s)}_{ex,\downarrow}) - i\Omega_{s,\mp}e^{-i\omega_s t}N^{p}_{ex,\uparrow(\downarrow)} - i\Omega_{p,\mp}e^{-i\omega_p t}N^{s}_{ex,\uparrow(\downarrow)}, \tag{18a}$$

$$\frac{\partial N^{(s)}_{ex,\uparrow(\downarrow)}}{\partial t} = -(\Gamma_1 + \Gamma_s)N^{(s)}_{ex,\uparrow(\downarrow)} + \Gamma_s N^{(s)}_{ex,\downarrow(\uparrow)} + 4\,\mathrm{Im}[\Omega^*_{s,\mp}e^{i\omega_s t}P^{(p)}_{ex,\uparrow(\downarrow)} + \Omega^*_{p,\mp}e^{i\omega_p t}P^{(s)}_{ex,\uparrow(\downarrow)}]. \tag{18b}$$

We apply the techniques of slowly varying variables again. However, this time, both the polarizations and population fluctuations corresponding to the signal have two frequency components:

$$P^{(s)}_{ex,\uparrow(\downarrow)} = \tilde{P}^{(s)}_{ex,\uparrow(\downarrow)}(\omega_s)e^{-i\omega_s t} + \tilde{P}^{(s)}_{ex,\uparrow(\downarrow)}(2\omega_p - \omega_s)e^{-i(2\omega_p - \omega_s)t}, \tag{19a}$$

$$N^{(s)}_{ex,\uparrow(\downarrow)} = \tilde{N}^{(s)}_{ex,\uparrow(\downarrow)}e^{-i\omega_s t} + \tilde{N}^{(s)*}_{ex,\uparrow(\downarrow)}e^{i\omega_s t}. \tag{19b}$$

For the terms $N^{(s)}_{ex,\uparrow(\downarrow)}$, although there are two frequency components in each of them, we only need one variable for each because the population fluctuations must be real. Equations (19a) and (19b) are substituted into Eqs. (18a) and (18b). For steady-state solutions, the comparison of the magnitude of each frequency component on the right-hand and the left-hand sides of Eqs. (18a) and (18b) results in a set of six-variable coupled equations. Several functions are defined to simplify the result:

$$D(\omega_s, \omega_p) = 2\left(\frac{1}{\omega_s - \omega_{ex} + i\Gamma_2^{(p)}} - \frac{1}{\omega_p - \omega_{ex} - i\Gamma_2^{(p)}}\right), \tag{20a}$$

$$F_{\pm}(\omega_s, \omega_p) = \omega_s - \omega_p + i(\Gamma_1 + 2\Gamma_s) + 2|\Omega_{p,\pm}|^2\left(\frac{1}{2\omega_p - \omega_s - \omega_{ex} - i\Gamma_2^{(p)}} - \frac{1}{\omega_s - \omega_{ex} + i\Gamma_2^{(p)}}\right), \tag{20b}$$

$$G_{\uparrow(\downarrow)}(\omega_s, \omega_p) = -\Gamma_s + 2\gamma|\Omega_{p,\mp}|^2 \times\left(\frac{H^*_{\uparrow(\downarrow)}(\omega_p)}{2\omega_p - \omega_s - \omega_{ex} - i\Gamma_2^{(p)}} + \frac{H_{\uparrow(\downarrow)}(\omega_p)}{\omega_s - \omega_{ex} + i\Gamma_2^{(p)}}\right). \tag{20c}$$

After a detailed calculation, the expressions for the slowly varying variables $\tilde{P}^{(s)}_{ex,\uparrow(\downarrow)}(\omega_s)$ are as follows:

$$\tilde{P}^{(s)}_{ex,\uparrow(\downarrow)}(\omega_s)=\frac{1}{\omega_s-\omega_{ex}+i\Gamma_2^{(p)}}\left\{N^{(p)}_{ex,\uparrow(\downarrow)}\Omega_{s,\mp}\left[1+\frac{D(\omega_s,\omega_p)|\Omega_{p,\mp}|^2\{[1-i\gamma H_{\uparrow(\downarrow)}(\omega_p)]F_{\pm}(\omega_s,\omega_p)+iG_{\downarrow(\uparrow)}(\omega_s,\omega_p)\}}{F_+(\omega_s,\omega_p)F_-(\omega_s,\omega_p)+i[F_-(\omega_s,\omega_p)G_{\downarrow}(\omega_s,\omega_p)+F_+(\omega_s,\omega_p)G_{\uparrow}(\omega_s,\omega_p)]}\right]\right.$$
$$\left.-iN^{(p)}_{ex,\downarrow(\uparrow)}\Omega_{s,\pm}\frac{D(\omega_s,\omega_p)\Omega^*_{p,\pm}\Omega_{p,\mp}[\gamma H_{\uparrow(\downarrow)}(\omega_p)F_{\mp}(\omega_s,\omega_p)+G_{\uparrow(\downarrow)}(\omega_s,\omega_p)]}{F_+(\omega_s,\omega_p)F_-(\omega_s,\omega_p)+i[F_-(\omega_s,\omega_p)G_{\downarrow}(\omega_s,\omega_p)+F_+(\omega_s,\omega_p)G_{\uparrow}(\omega_s,\omega_p)]}\right\}. \tag{21}$$

For the case $|\Omega_{p,+}|=|\Omega_{p,-}|$, such as a linearly polarized pump, Eq. (21) can be simplified by the following auxiliary equations:

$$|\Omega_{p,+}|=|\Omega_{p,-}|\equiv|\Omega_p|, \tag{22a}$$

$$N^{(p)}_{ex,\uparrow}=N^{(p)}_{ex,\downarrow}\equiv N^{(p)}_{ex}/2, \tag{22b}$$

$$H_{\uparrow}(\omega_p)=H_{\downarrow}(\omega_p)\equiv H(\omega_p), \tag{22c}$$

$$F_+(\omega_s,\omega_p)=F_-(\omega_s,\omega_p)\equiv F(\omega_s,\omega_p), \tag{22d}$$

$$G_{\uparrow}(\omega_s,\omega_p)=G_{\downarrow}(\omega_s,\omega_p)\equiv G(\omega_s,\omega_p). \tag{22e}$$

We note that the dot product $\mathbf{E}_s\cdot\mathbf{E}_p^*$ can be rewritten as follows:

$$\mathbf{E}_s\cdot\mathbf{E}_p^*=E_{s,+}E^*_{p,+}+E_{s,-}E^*_{p,-}. \tag{23}$$

We will only focus on the linear response of the signal. The FWM term will be dropped. Denote the linear electric polarization density in real space generated by the signal as $\mathbf{P}_s(\omega_s)$. With the aid of Eqs. (22a)–(22d) and (23), we substitute Eq. (21) into Eq. (5) and obtain the linear electric polarization density of the signal $\mathbf{P}_s(\omega_s)$ as follows:

$$\mathbf{P}_s(\omega_s)=\frac{|I_{ch}er_{ch}|^2|\Phi_{ex}(\boldsymbol{\rho}=\mathbf{0})|^2}{2\hbar L_z}\frac{N^{(p)}_{ex}}{\omega_s-\omega_{ex}+i\Gamma_2^{(p)}}e^{-i\omega_s t}$$
$$\times\left\{\left[1+\frac{|\Omega_p|^2D(\omega_s,\omega_p)}{F(\omega_s,\omega_p)}\right]\frac{\mathbf{E}_s}{2}\right.$$
$$-i\frac{2|\Omega_p|^2D(\omega_s,\omega_p)[\gamma H(\omega_p)F(\omega_s,\omega_p)+G(\omega_s,\omega_p)]}{F(\omega_s,\omega_p)[F(\omega_s,\omega_p)+2iG(\omega_s,\omega_p)]}$$
$$\left.\times\left(\frac{\mathbf{E}_s}{2}\cdot\hat{e}_p^*\right)\hat{e}_p\right\}. \tag{24}$$

Assume that both the signal and pump are linearly polarized. From Eq. (24), this linearly polarized pump results in anisotropy in the QW plane. The signal electric field must be decomposed into the component parallel to the pump polarization as well as the one perpendicular to it. Two components will generate two different linear electric polarization densities and thus experience different permittivities. If the parameters γ and Γ_s describing EID and spin flip both vanish, respectively, the function $G(\omega_s,\omega_p)$ also vanishes. Thus the second term proportional to $\mathbf{E}_s\cdot\hat{e}_p$ will not be present. The system will be isotropic in the QW plane no matter what the configuration of the signal and pump polarizations is. Therefore EID and spin flip play the roles in transforming a uniaxial system into a biaxial one.

Assume that the pump polarization is polarized along the x axis, $\hat{e}_p=\hat{x}$, and we write the components of the signal in the form of a column vector. For the signal, the generated linear electric displacement density $\mathbf{D}_s(\omega_s)$ is related to its linear electric polarization density as follows:

$$\mathbf{D}_s(\omega_s)=\epsilon_0\epsilon_{\mathrm{bgd}}\bar{\bar{I}}\cdot\frac{\mathbf{E}_s}{2}e^{-i\omega_s t}+\mathbf{P}_s(\omega_s)=\epsilon_0\bar{\bar{\epsilon}}^L_s(\omega_s)\cdot\frac{\mathbf{E}_s}{2}e^{-i\omega_s t}, \tag{25a}$$

$$\mathbf{E}_s=\begin{pmatrix}E_s^{(x)}\\E_s^{(y)}\end{pmatrix}, \tag{25b}$$

where $\bar{\bar{I}}$ is the two-by-two identity matrix, ϵ_0 is the vacuum permittivity, ϵ_{bgd} is the relative background permittivity, and $\bar{\bar{\epsilon}}^L_s(\omega_s)$ is the linear relative permittivity tensor experienced by the signal. The explicit expression of $\bar{\bar{\epsilon}}^L_s(\omega_s)$ is then as follows:

$$\bar{\bar{\epsilon}}^L_s(\omega_s)=\begin{pmatrix}\epsilon_s^{(x)}(\omega_s)&0\\0&\epsilon_s^{(y)}(\omega_s)\end{pmatrix}=\begin{pmatrix}\epsilon_{\mathrm{bgd}}&0\\0&\epsilon_{\mathrm{bgd}}\end{pmatrix}+\frac{|I_{ch}er_{ch}|^2|\Phi_{ex}(\boldsymbol{\rho}=\mathbf{0})|^2}{2\hbar L_z\epsilon_0}\frac{N^{(p)}_{ex}}{\omega_s-\omega_{ex}+i\Gamma_2^{(p)}}$$
$$\times\begin{pmatrix}1+\dfrac{|\Omega_p|^2D(\omega_s,\omega_p)[1-2i\gamma H(\omega_p)]}{F(\omega_s,\omega_p)+2iG(\omega_s,\omega_p)}&0\\0&1+\dfrac{|\Omega_p|^2D(\omega_s,\omega_p)}{F(\omega_s,\omega_p)}\end{pmatrix}. \tag{26}$$

III. THEORETICAL RESULTS AND COMPARISON WITH EXPERIMENTS

Because the analytical solutions of the linear relative permittivities for the two polarizations are available, we can utilize them to calculate the real part of the refractive index $\mathrm{Re}[n_s^{x(y)}(\omega_s)]$ and the absorption $A_s^{x(y)}(\omega_s)$ of the signal as a function of the detuning $(\omega_s-\omega_p)/2\pi$. Furthermore, from the real part of the refractive index, we can calculate the slow-down factor $R_s^{x(y)}(\omega_s)$, which is the ratio of speed of light in free space to the group velocity of a signal wave packet with center frequency ω_s in the QW in the presence of the excitonic population oscillation caused by the pump-signal beating. The refractive indices, the absorptions, and the slow-down factors of the signals polarized at the two orthogonal directions are as follows:

$$n_s^{x(y)}(\omega_s)=\sqrt{\epsilon_s^{x(y)}(\omega_s)}, \tag{27a}$$

$$A_s^{x(y)}(\omega_s)=2\frac{\omega_s}{c}\mathrm{Im}[n_s^{x(y)}(\omega_s)], \tag{27b}$$

$$R_s^{x(y)}(\omega_s)=\mathrm{Re}[n_s^{x(y)}(\omega_s)]+\omega_s\frac{\partial\,\mathrm{Re}[n_s^{x(y)}(\omega_s)]}{\partial\omega_s}. \tag{27c}$$

We have simulated the transmission spectra by taking the variation of the refractive index and absorption in the QW region into account. The simulation shows that extracted absorbance in the experiment[15] can be directly treated as the single-pass absorbance in the QW region. We use the following parameters for our theoretical calculations and fittings to some of the experimental data. The excitonic energy $\hbar\omega_{ex}$ is 1.5358 eV. The photon energy of the pump $\hbar\omega_p$ is the same as the excitonic energy. The magnitude of the variational 1*s* excitonic in-plane wave function of the relative coordinate at the origin $|\Phi_{ex}(\mathbf{0})|^2$ is 3.18×10^{-5} Å^{-2}. The bulk dipole moment er_{ch} is 6.45 *e*Å. The relaxation constant Γ_1 is 2.5133 ns^{-1}. The spin-flip constant Γ_s is set to 50 ps due to the exchange effect of holes and electrons in intrinsic materials after Ref. 29. The intrinsic dephasing constant $\Gamma_2^{(0)}$ is 0.4716 ps^{-1}. The EID parameter γ is 2.24 ps^{-1}. The relative background permittivity ϵ_{bgd} is 12.25. The sample used in the experiment consists of 15 GaAs/$Al_{0.3}Ga_{0.7}$As QWs. The barrier width between two QWs is 150 Å. The width of each QW is 135 Å. The effective length of the absorption region L_{eff} is thus 15×135 Å$=2025$ Å.

Figure 3(a) shows the calculated absorbance spectra for the parallel-polarization configuration under different pump intensities. This calculation is performed by matching the background saturated absorption and magnitude of the depth under the variations of pump intensities as well as the parameters Γ_1, $\Gamma_2^{(0)}$, and γ. The absorbance spectrum is the product of the absorption spectrum and the effective length of the absorption region. The corresponding real parts of the refractive index are shown in Fig. 3(b). As the pump intensity is increased, the background absorbance is gradually saturated due to power-broadening. When the signal detuning is roughly within the range of the population relaxation

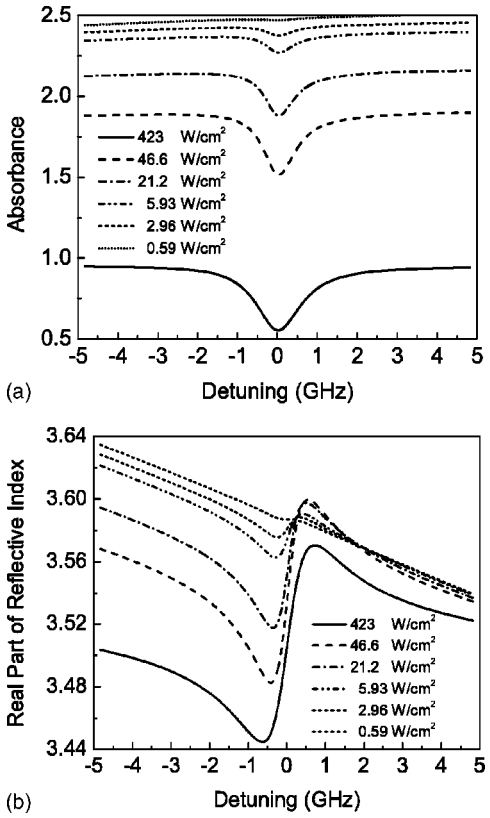

FIG. 3. Parallel-polarization configuration between the signal and the pump polarization. (a) The calculated absorbance spectra and (b) the real part of the refractive indices of the optical signal are plotted as a function of the detuning frequency between the signal and pump.

constant Γ_1, an absorption dip is created. For direct-band-gap semiconductors, the spectral widths are about a few gigahertzs. The width of the dip also gets broadened as the pump intensity is increased. The ratio between the depth and background saturated absorbance increases as the pump intensity gets higher. However, theoretically, the real depth of the dip has a maximum at a certain pump intensity. From the Kramers-Kronig relation due to the causality of linear responses, the real part of the refractive index corresponding to the absorption dip must have a rapid increase as the frequency of the signal increases. In Fig. 3(b), the slope of the real part of the refractive index at zero detuning first increases as the pump intensity gets higher, which reflects the increase of the depth of the dip. However, two factors stop the increase of the slope at high pump intensity. The first one is the increase of the spectral width of the dip as the pump intensity gets higher. This will broaden the range in which the fast variation of the real part of the refractive index takes place and thus reduces the slope. The second one is the saturated background absorption limiting the absolute depth of the dip. The variation of the real part of the refractive index will be subjected to this saturation and result in the decrease of the slope.

Besides the rapid change of refractive index in a local frequency range, the global offset of the refractive index also varies as the pump intensity changes. Theoretically, if the

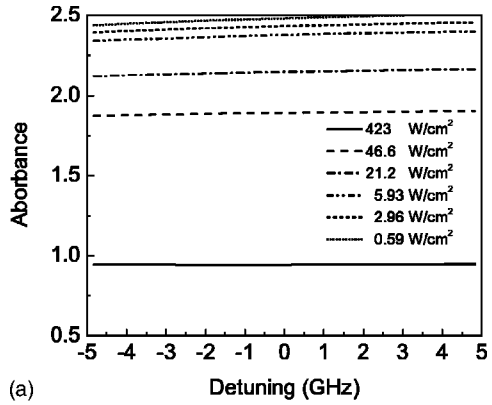

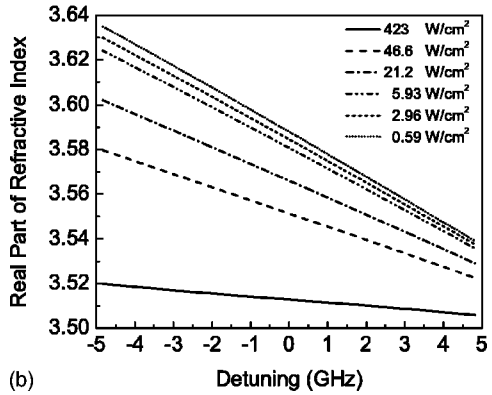

FIG. 4. Orthogonal-polarization configuration between the signal and the pump polarization. (a) The calculated absorption spectra and (b) the real part of the refractive indices of the optical signal are plotted as a function of the detuning frequency between the signal and pump.

change of dielectric constant caused by the optical transition is small compared with the background dielectric constant, the offset should remain constant as the pump increases. This constant will reflect the background dielectric constant only. On the other hand, if the change of the dielectric constant is significant enough, this offset will be modified by the change or dielectric constant itself. For excitonic population oscillation, because a large and rapid change is created in a narrow frequency range, there is no guarantee for the constancy of this offset.

The presence of EID and spin flip break the isotropy in the QW plane and makes the phenomena for orthogonal-polarization configuration completely different from those of the parallel-polarization one. Figures 4(a) and 4(b) show the counterparts in Fig. 3. There are significant differences between the two configurations. The absorption dip of the orthogonal-polarization configuration is unobservable. The flat absorbance in this narrow frequency range is caused by the relative phase between the two population pulsations of the two subsystems. The positive-helicity and negative-helicity components of the signal have distinct phase differences from their counterparts of the pump. For the parallel-polarization configuration, we have the following equations for the signal-pump phase differences $\angle E_{s,\pm} - \angle E_{p,\pm}$:

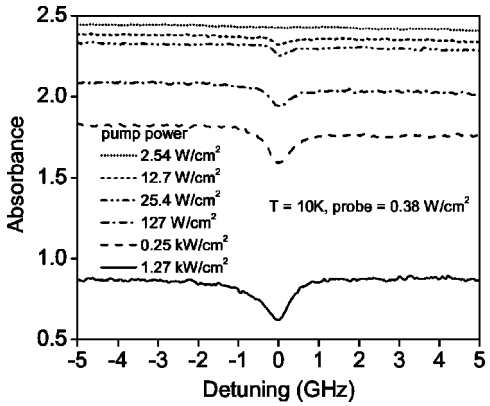

FIG. 5. Experimental results of the absorbance due to excitonic population oscillation in GaAs/AlGaAs quantum wells, which should be compared with the theory curves in Fig. 3(a).

$$(\angle E_{s,-} - \angle E_{p,-}) - (\angle E_{s,+} - \angle E_{p,+}) = 0. \qquad (28a)$$

On the other hand, for orthogonal-polarization configuration, we have

$$(\angle E_{s,-} - \angle E_{p,-}) - (\angle E_{s,+} - \angle E_{p,+}) = \pi. \qquad (28b)$$

For the orthogonal-polarization configuration, the two induced positive-frequency components of the population pulsations $\tilde{N}^{(s)}_{ex,\uparrow(\downarrow)}$, which have the phase following $\angle E_{s,\mp} - \angle E_{p,\mp}$ when EID and spin flip are not present, will oscillate out of phase, and so are the negative-frequency components. If EID is included, these out-of-phase oscillations of the effective population differences will cancel each other. There will be no extra contribution to linear electric polarization density from the pulsations of dephasing terms. The presence of spin flip is also a mechanism killing the coherent population oscillation in orthogonal-polarization configuration. The fast population exchange tends to bring the effective population differences of the two spin ensembles close to each other and hence significantly suppresses the magnitude of the population variations when the two effective population differences oscillate out of phase. On the other hand, for the parallel-polarization configuration, the contributions from the two population oscillations tend to add in phase and thus enable the observation of significant dips. Also, spin flip is not a problem in parallel-polarization configuration because the two effective population differences oscillate in phase and are always close to each other at any moment. This can be easily checked by the observation that the x component of the permittivity tensor in Eq. (26) does not depend on spin-flip constant Γ_s. The argument of EID has been applied to the generated FWM signals in semiconductor quantum structures and can account for the polarization-dependent phenomena qualitatively.[24,25]

Figure 5 shows the experimental data on excitonic population oscillation for parallel-polarization configuration.[15] It should be compared with the theory curves in Fig. 3(a). In the experiment, a single-mode Ti-sapphire laser provides the continuous-wave pump while a tunable diode laser works as

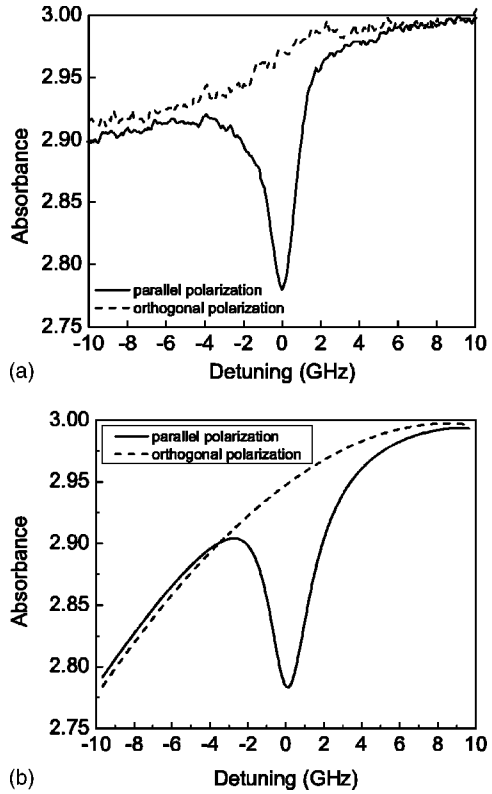

FIG. 6. (a) Experimental results of the polarization dependence of the absorbance spectrum in the presence of excitonic population oscillation. The experiment was done near the excitonic absorption peak. (b) Our theoretical results.

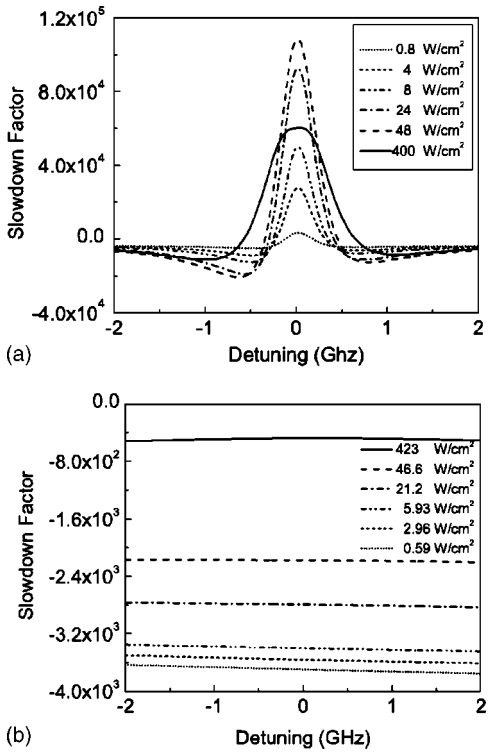

FIG. 7. The slowdown factor of the excitonic population oscillation (a) when $\hat{e}_s \| \hat{e}_p$ and (b) when $\hat{e}_s \perp \hat{e}_p$ are plotted as a function of the detuning frequency between the signal and pump.

the signal. For details, please refer to Ref. 15. The pumping intensities for the fitting are set as 0.00059, 0.00298, 0.00593, 0.0212, 0.0466, and 0.423 kW/cm^2. They are chosen to match the background saturated absorbance. The actual pump intensities in the experiment are 0.00254, 0.0127, 0.0254, 0.127, 0.25, and 1.25 kW/cm^2. The intensities used in theoretical fitting are about one-third or one-fifth of the experimental values. The discrepancy may result from the fact that the actual pump intensity entering the absorption region is not so high as the estimated intensity outside the sample. Compared with experiment, the theoretical fitting tends to overestimate the depth of the dips. It may be due to the neglect of several factors in our models including the phase-space filling and the reduction of oscillation strength due to electron-hole plasma screening.

Figure 6(a) shows another experimental measurement of the absorbance corresponding to the two different polarization configurations at a certain pump intensity. Figure 6(b) shows the corresponding theoretical results. The experiment was done near the excitonic absorption peak. We use the relaxation constant $\Gamma_1 = 7.79$ ns^{-1} and the intrinsic dephasing constant $\Gamma_2^{(0)} = 0.37$ ps^{-1}. The pump intensity is 0.019 kW/cm^2, and the parameter γ describing EID is 1.76 ps^{-1}. The absorption dip vanishes in the orthogonal-polarization configuration. Theoretically, it will be hard to observe coherent absorption dip for orthogonal-polarization configuration due to EID and spin flip.

Figures 7(a) and 7(b) show the theoretical slowdown factors corresponding to Figs. 3 and 4 for the signal as a function of its center frequency. For parallel-polarization configuration, the rapid variation of the real part of the refractive index has a positive slope with respect to the signal frequency and can give rise to a significant slowdown of the wave packets whose main frequency components lie within the frequency range of the dip. Other parts with negative slope will cause superluminal phenomena of the wave packets and are not our main concern here. A rule of thumb is that the narrower and the deeper the dip, the higher the peak slowdown factor. For the parallel-polarization configuration, the extra contribution from the EID can still result in a significant slowdown factor. The magnitude of the slowdown factor is of the order of 10^4. However, for the orthogonal-polarization configuration, the out-of-phase cancellations of the two population oscillations due to EID and spin flip eliminate the dip in the absorbance spectra. No significant slowdown factor of the wave packet is present. Only the superluminal phenomena due to the saturated background absorption can be observed.

Figure 8(a) shows the experimental result of the phase delay of the signal $\Delta P^{x(y)}(\omega_s)$ and the corresponding absorbance as a function of detuning for the parallel-polarization configuration. The phase delay of the signal optical field describes the variation of the real part of the refractive index when the pump is present. It is described by the following equation:

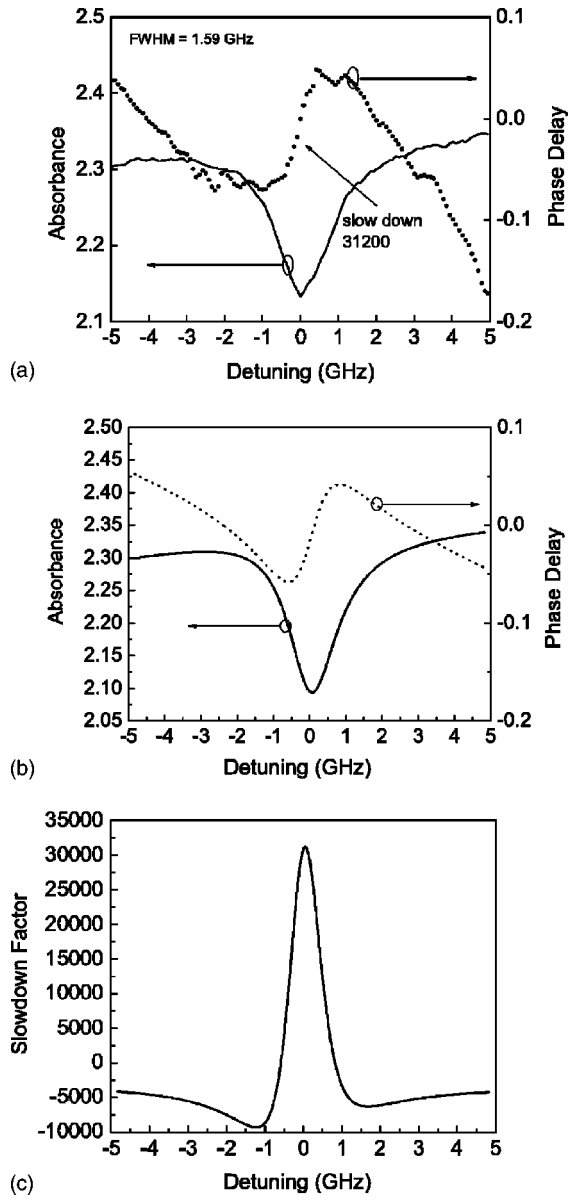

FIG. 8. (a) Experimental results of the phase delay and absorbance due to excitonic population oscillation in GaAs/AlGaAs quantum wells. (b) Our theoretical result. (c) The theoretical slowdown factor as a function of the detuning frequency between the signal and pump. The peak slowdown factor agrees with the value extracted from the experiment.

$$\Delta P^{x,(y)}(\omega_s) = \frac{\omega_s}{c}\,\mathrm{Re}[n^{x(y)}(\omega_s)]L_{\mathrm{eff}} + a, \tag{29}$$

where a is an arbitrary constant. In the experiment, the measurement was carried out by a Mach-Zehnder interferometer.[15] From this phase difference, we can extract the variation of the real part of the refractive index and estimate the slowdown factor. Figure 8(b) shows the theoretical result for the corresponding experiment. We use the relaxation constant $\Gamma_1 = 4.65\ \mathrm{ns}^{-1}$, and the intrinsic dephasing constant $\Gamma_2^{(0)} = 0.448\ \mathrm{ps}^{-1}$. The pump intensity is $0.028\ \mathrm{kW/cm}^2$, and the parameter γ describing EID is $2.1299\ \mathrm{ps}^{-1}$. The constant

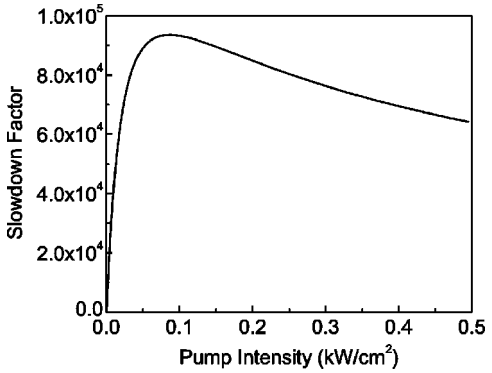

FIG. 9. Peak slowdown factor as a function of pump intensity.

a has been adjusted to match the experimental result. The shape and magnitude of the phase delay and absorbance agree well with those obtained from the experiment. Figure 8(c) shows the calculated slowdown factor from our theoretical results. The peak slowdown factor is about 3.13×10^4, which agrees well with the value 3.12×10^4 from the experiment.

Figure 9 shows the peak slowdown factor of the parallel-polarization configuration as a function of the pump intensity. Due to the broadening of the spectral width and the saturation of the overall excitonic absorption, there is an optimal pump intensity that maximizes the peak slowdown factor. The optimized peak slowdown factor can be as high as 9.4×10^4. The experiment corresponding to Fig. 5 also confirms the magnitude of this slowdown factor.[15]

IV. CONCLUSION

We use an atomiclike model extended from semiconductor Bloch equations to describe the phenomena of excitonic population oscillation in QW for two spin subsystems coupled by EID. Given a reasonable recombination lifetime, a significant but narrow absorption dip can be observed. The corresponding slowdown factor can be close to 10^5. However, depending on the polarization configurations of the pump and signal, the in-phase and out-of-phase population oscillations will result in completely different absorption spectra. The unobservable dip for the orthogonal-polarization configuration implies insignificant slowdown compared with that of the parallel-polarization configuration. We also show theoretical results for the absorbance and refractive index spectra of the signal in the presence of population oscillation caused by the signal-pump beating. Our theoretical results of the absorbance spectra and slowdown factor agree very well with the experimental data and their polarization dependence.

ACKNOWLEDGMENTS

We thank Tao Li and F. Sedgwick for the technical discussion. This work at the University of Illinois and University of California at Berkeley was supported by DARPA under Grant No. AFSA3631-22549.

*Electronic address: s-chuang@uiuc.edu

[1] A. Kasapi, M. Jain, G. Y. Yin, and S. E. Harris, Phys. Rev. Lett. **74**, 2447 (1995).
[2] O. Schmidt, R. Wynands, Z. Hussein, and D. Meschede, Phys. Rev. A **53**, R27 (1996).
[3] L. V. Hau, S. E. Harris, Z. Dutton, and C. H. Behroozi, Nature (London) **397**, 594 (1999).
[4] M. M. Kash, V. A. Sautenkov, A. S. Zibrov, L. Hollberg, G. R. Welch, M. D. Lukin, Y. Rostovtsev, E. S. Fry, and M. O. Scully, Phys. Rev. Lett. **82**, 5229 (1999).
[5] D. Budker, D. F. Kimball, S. M. Rochester, and V. V. Yashchuk, Phys. Rev. Lett. **83**, 1767 (1999).
[6] A. V. Turukhin, V. S. Sudarshanam, M. S. Shahriar, J. A. Musser, B. S. Ham, and P. R. Hemmer, Phys. Rev. Lett. **88**, 023602 (2002).
[7] M. S. Bigelow, N. N. Lepeshkin, and R. W. Boyd, Phys. Rev. Lett. **90**, 113903 (2003).
[8] M. Sargent III, Phys. Rep. **43**, 223 (1978).
[9] R. W. Boyd, M. G. Raymer, P. Narum, and D. J. Harter, Phys. Rev. A **24**, 411 (1981).
[10] B. Mollow, Phys. Rev. **188**, 1969 (1969).
[11] B. Mollow, Phys. Rev. A **5**, 2217 (1972).
[12] G. P. Agrawal, J. Opt. Soc. Am. B **5**, 147 (1988).
[13] A. E. Paul, M. Lindberg, S. An, M. Sargent III, and S. W. Koch, Phys. Rev. A **42**, 1725 (1990).
[14] F. L. Zhou, M. Sargent III, S. W. Koch, and W. W. Chow, Phys. Rev. A **41**, 463 (1990).
[15] P.-C. Ku, P. Palinginis, T. Li, F. Sedgwick, S.-W. Chang, H. Wang, C. J. Chang-Hasnain, and S.-L. Chuang (unpublished).
[16] E. Conwell and V. F. Weisskopf, Phys. Rev. **77**, 388 (1950).
[17] E. M. Conwell and M. O. Vassell, Phys. Rev. **166**, 797 (1968).
[18] D. Ahn and S. L. Chuang, Phys. Rev. B **37**, 2529 (1988).
[19] W. A. Harrison, Phys. Rev. **104**, 1281 (1956).
[20] D. Bohm and D. Pines, Phys. Rev. **92**, 609 (1953).
[21] L. C. Andreani, Solid State Commun. **77**, 641 (1991).
[22] V. Srinivas, J. Hryniewicz, Y. J. Chen, and C. E. C. Wood, Phys. Rev. B **46**, 10193 (1992).
[23] J. Martinez-Pastor, A. Vinattieri, L. Carraresi, M. C. P. Roussignol, and G. Weimann, Phys. Rev. B **47**, 10456 (1993).
[24] H. Wang, K. Ferrio, D. G. Steel, Y. Z. Hu, R. Binder, and S. W. Koch, Phys. Rev. Lett. **71**, 1261 (1993).
[25] H. Wang, K. B. Ferrio, D. G. Steel, P. R. Berman, Y. Z. Hu, R. Binder, and S. W. Koch, Phys. Rev. A **49**, R1551 (1994).
[26] Y. Z. Hu, R. Binder, S. W. Koch, S. T. Cundiff, H. Wang, and D. G. Steel, Phys. Rev. B **49**, 14382 (1994).
[27] A. Tackeuchi, S. Muto, T. Inata, and T. Fujii, Appl. Phys. Lett. **56**, 2213 (1990).
[28] T. C. Damen, K. Leo, J. Shah, and J. E. Cunningham, Appl. Phys. Lett. **58**, 1902 (1991).
[29] T. C. Damen, L. V. Na, J. E. Cunningham, J. Shah, and L. J. Sham, Phys. Rev. Lett. **67**, 3432 (1991).
[30] M. Lindberg and S. W. Koch, Phys. Rev. B **38**, 3342 (1988).
[31] H. Haug and S. W. Koch, *Quantum Theory of the Optical and Electronic Properties of Semiconductors* 3rd ed. (World Scientific, Singapore, 1994).
[32] D. A. B. Miller, D. S. Chemla, T. C. Damen, A. C. Gossard, W. Wiegmann, T. H. Wood, and C. A. Burrus, Phys. Rev. B **32**, 1043 (1985).
[33] H. Haug and S. Schmitt-Rink, Prog. Quantum Electron. **9**, 3 (1984).